Inorg. Chem. **2003**, *42*, 7959–7966

$RE_2MAl_6Si_4$ (RE = Gd, Tb, Dy; M = Au, Pt): Layered Quaternary Intermetallics Featuring $CaAl_2Si_2$-Type and $YNiAl_4Ge_2$-Type Slabs Grown from Aluminum Flux

Susan E. Latturner,[†] Daniel Bilc,[‡] S. D. Mahanti,[‡] and Mercouri G. Kanatzidis*[,†]

Department of Chemistry and Department of Physics, Michigan State University, East Lansing, Michigan 48824

Received June 9, 2003

Six new intermetallic aluminum silicides—$Gd_2PtAl_6Si_4$, $Gd_2AuAl_6Si_4$, $Tb_2PtAl_6Si_4$, $Tb_2AuAl_6Si_4$, $Dy_2PtAl_6Si_4$, and $Dy_2AuAl_6Si_4$—have been obtained from reactions carried out in aluminum flux. The structure of these compounds was determined by single-crystal X-ray diffraction. They form in space group $R\bar{3}m$ with cell constants of $a = 4.1623(3)$ Å and $c = 51.048(5)$ Å for the $Gd_2PtAl_6Si_4$ compound. The crystal structure is comprised of hexagonal nets of rare earth atoms alternating with two kinds of layers that have been observed in other multinary aluminide intermetallic compounds ($CaAl_2Si_2$ and $YNiAl_4Ge_2$). All six $RE_2MAl_6Si_4$ compounds show antiferromagnetic transitions at low temperatures ($T_N < 20$ K); magnetization studies of the Dy compounds show metamagnetic behavior with reorientation of spins at 6000 G. Band structure calculations indicate that the AlSi puckered hexagonal sheets in this structure are electronically distinct from the other surrounding structural motifs.

Introduction

Polar intermetallic compounds have garnered much attention recently due to their intermediate nature between charge-balanced Zintl phases and fully delocalized metal alloys. The structures of such materials are not bound by simple electron counting rules and often involve complex layers and/or networks.[1] Rare-earth-containing intermetallic compounds often feature isolated ionic rare earth magnetic moments unaffected by the conduction electrons of the rest of the structure. Despite being completely comprised of metallic elements, a certain amount of charge transfer in compounds such as $RuAl_2$ and Fe_2VAl produces small band gaps resulting in semiconducting behavior.[2] Characteristics such as mixed valence and superconductivity have also been observed in polar intermetallics.

In addition to possessing complex structures and intriguing electronic properties, aluminide intermetallics play an important role in the behavior of aluminum alloys. Other elements such as silicon and transition metals are added to aluminum to improve the properties of the resulting alloy. This causes the formation of multinary aluminide phases within the bulk aluminum matrix.[3] These adventitious compounds can improve or degrade the physical properties of the bulk material; study of these phases is therefore important. The combination of several elements in liquid aluminum, a model for the formation and processing of aluminum alloys, has resulted in many new structures such as $YNiAl_4Ge_2$,[4] $Sm_2Ni(Ni_xSi_{1-x})Al_4Si_6$,[5] $RE_4Fe_{2+x}Al_{7-x}Si_8$,[6] and $RE_8Ru_{12}Al_{49}Si_9(Al_xSi_{12-x})$.[7]

In this work, a new layered quaternary structure, $RE_2MAl_6Si_4$, has been obtained from the combination of a rare earth metal (RE = Gd, Tb, Dy) and a noble metal (M = gold or platinum) in silicon-rich aluminum solution. The reactions

* To whom correspondence should be addressed. E-mail: kanatzid@cem.msu.edu.
† Department of Chemistry.
‡ Department of Physics.

(1) *CRC Handbook of Crystal Structures and Magnetic Properties of Rare Earth Intermetallics*; CRC Press: Boca Raton, FL, 1994. (b) Haussermann, U.; Amerioun, S.; Eriksson, L.; Leen, C.; Miller, G. *J. Am. Chem. Soc.* **2002**, *124*, 4371−4383.
(2) Weinert, M.; Watson, R. E. *Phys. Rev. B* **1998**, *58*, 9732−9740.
(3) Suresh, S.; Mortensen, A.; Needleman, A. *Fundamentals of Metal Matrix Composites*; Butterworth-Heinemann: Boston, MA, 1993.
(4) Sieve, B.; Chen, X.; Cowen, J.; Larson, P.; Mahanti, S. D.; Kanatzidis, M. G. *Chem. Mater.* **1999**, *11*, 2451−2455.
(5) Chen, X. Z.; Sportouch, S.; Sieve, B.; Brazis, P.; Kannewurf, C. R.; Cowen, J. A.; Patschke, R.; Kanatzidis, M. G. *Chem. Mater.* **1998**, *10*, 3202−3211.
(6) Sieve, B.; Sportouch, S.; Chen, X. Z.; Cowen, J. A.; Brazis, P.; Kannewurf, C. R.; Papaefthymiou, V.; Kanatzidis, M. G. *Chem. Mater.* **2001**, *13*, 273−283.
(7) Sieve, B.; Chen, X. Z.; Henning, R.; Brazis, P.; Kannewurf, C. R.; Cowen, J. A.; Schultz, A. J.; Kanatzidis, M. G. *J. Am. Chem. Soc.* **2001**, *123*, 7040−7047.

10.1021/ic0346432 CCC: $25.00
Published on Web 10/31/2003

Table 1. Crystallographic Data for $RE_2MAl_6Si_4$

	$Gd_2PtAl_6Si_4$ (**1**)	$Gd_2AuAl_6Si_4$ (**2**)	$Tb_2PtAl_6Si_4$ (**3**)	$Tb_2AuAl_6Si_4$ (**4**)	$Dy_2PtAl_6Si_4$ (**5**)	$Dy_2AuAl_6Si_4$ (**6**)
fw	783.83	785.71	787.17	789.05	794.34	796.21
space group	$R\bar{3}m$	$R\bar{3}m$	$R\bar{3}m$	$R\bar{3}m$	$R\bar{3}m$	$R\bar{3}m$
a (Å)	4.1623(3)	4.1749(8)	4.1547(5)	4.1837(3)	4.150(1)	4.1901(6)
c (Å)	51.048(5)	50.59(1)	50.993(9)	50.454(4)	50.64(2)	50.29(1)
V (Å^3)	765.91	763.68	762.29	764.80	755.35	764.62
Z	3	3	3	3	3	3
calcd density (g/cm^3)	5.098	5.125	5.144	5.140	5.239	5.188
temp (K)	173	295	295	295	173	173
$2\theta_{max}$ (deg)	55.97	75.13	74.43	74.48	56.34	56.52
μ (mm^{-1})	27.42	18.78	28.42	28.99	9.76	19.86
Index ranges	$-5 \le h \le 5$	$-6 \le h \le 7$	$-6 \le h \le 7$	$-7 \le h \le 6$	$-5 \le h \le 5$	$-5 \le h \le 5$
	$-5 \le k \le 5$	$-7 \le k \le 7$	$-6 \le k \le 7$	$-7 \le k \le 7$	$-5 \le k \le 5$	$-5 \le k \le 5$
	$-66 \le l \le 66$	$-85 \le l \le 85$	$-85 \le l \le 85$	$-83 \le l \le 81$	$-60 \le l \le 64$	$-64 \le l \le 64$
reflcns collcd	2634	4043	3953	4026	2547	2540
unique reflcns	300	561	548	553	297	302
R indices ($I > 2\sigma$(I))	$R_1 = 0.0241$	$R_1 = 0.0213$	$R_1 = 0.0229$	$R_1 = 0.0171$	$R_1 = 0.0212$	$R_1 = 0.0212$
	$wR_2 = 0.0596$	$wR_2 = 0.0453$	$wR_2 = 0.0479$	$wR_2 = 0.0355$	$wR_2 = 0.0530$	$wR_2 = 0.0490$
R indices (all data)	$R_1 = 0.0294$	$R_1 = 0.0264$	$R_1 = 0.0362$	$R_1 = 0.0206$	$R_1 = 0.0232$	$R_1 = 0.0239$
	$wR_2 = 0.0609$	$wR_2 = 0.0467$	$wR_2 = 0.0507$	$wR_2 = 0.0362$	$wR_2 = 0.0535$	$wR_2 = 0.0499$
max peak and hole (e/Å)	1.52, −1.84	2.35, −3.32	2.36, −2.11	1.44, −1.39	1.38, −1.43	1.21, −1.44

[a] $R_1 = \sum||F_o| - |F_c||/\sum|F_o|$; $wR_2 = [\sum w\{|F_o| - |F_c|\}^2/\sum w|F_o|^2]^{1/2}$, $w = 1/\sigma^2\{|F_o|\}$.

studied here indicate that the presence of late rare-earth elements within a concentrated solution of Si in Al promotes the formation of compounds with puckered hexagonal AlSi sheets as structural motifs.

Experimental Procedure

Synthesis. In a nitrogen-filled glovebox, the rare-earth element, transition metal, aluminum pellets, and silicon powder were combined in various ratios in alumina crucibles. The initial exploratory ratio was 1 mmol of rare earth metal:1 mmol of transition metal:10 mmol of aluminum:5 mmol of silicon. The materials used were Gd, Tb, or Dy metal powder (Cerac, 99.9%), Au shavings from a gold coin (99.99%), Pt pieces from a platinum crucible (99.99%), aluminum pellets (Cerac, 99.99%), and silicon powder (Cerac, 99.96%). Each loaded crucible was placed into a fused silica tube, which was then sealed under a vacuum of 10^{-4} Torr. The samples were heated to 1000 °C in 12 h, held at this temperature for 30 h, and then cooled to 860 °C in 30 h. They were annealed at 860 °C for 60 h and then slowly cooled to room temperature in 3 days. The aluminum flux was removed by soaking the crucible in 5 M NaOH for 1 day. Single crystals were selected from the remaining solid for elemental analysis, X-ray diffraction, and magnetic susceptibility measurements.

EDS Analysis. Selected crystals were affixed to a SEM plate using carbon tape. Microprobe analysis of these samples was performed using a JEOL JSM-35C scanning electron microscope equipped with a Tracor Northern energy dispersive spectroscopy (EDS) detector. Data were acquired using a 20 kV accelerating voltage and an accumulation time of 50 s. In the analysis of numerous crystals from these reactions, a consistent rare earth: transition metal:Al:Si elemental ratio of 2:1:5 ± 1:4 was obtained. The relatively large range of the aluminum EDS data and its low value compared to that in the elemental ratio determined by X-ray diffraction is a common occurrence.

X-ray Crystallography. Single-crystal X-ray diffraction data for the six quaternary compounds were collected on a Bruker AXS SMART CCD diffractometer. Data processing was then performed using the program SAINT.[8] The three structures were refined using direct methods with the SHELXTL package of programs; absorption correction was carried out using SADABS.[9] Initial refinement of the structure solution was carried out with aluminum atoms in all Al and Si sites. On the basis of similarities to known structure types and bond length analysis, the capping sites of the layers were then assigned as Si atoms. Although this was not expected to affect the R value due to the almost identical electron density of Al and Si, the R value was lowered by the substitution (from 0.0174 to 0.0171 in the $Tb_2AuAl_6Si_4$ analogue, for instance) and the thermal parameters became more reasonable. The resulting stoichiometry agrees well with the elemental analysis from EDS. Data collection and refinement parameters for all six structures can be found in Table 1. Atomic positions and thermal parameters for $Gd_2PtAl_6Si_4$ as an example are listed in Table 2. Selected bond lengths for each compound are shown in Table 3.

Table 2. Atomic Positions and Equivalent Isotropic Displacement Parameters for $Gd_2PtAl_6Si_4$

atom	Wyckoff posn	x	y	z	U_{eq} [a]
Gd	6c	1/3	2/3	0.10030(1)	0.0065(3)
Pt	3a	0	0	0	0.0069(3)
Si(1)	6c	0	0	0.13524(8)	0.0075(8)
Si(2)	6c	2/3	1/3	0.06680(8)	0.0065(8)
Al(1)	6c	2/3	1/3	0.14820(9)	0.0086(9)
Al(2)	6c	0	0	0.04966 (9)	0.0076(9)
Al(3)	6c	2/3	1/3	0.01498 (9)	0.0080(9)

[a] U_{eq} is defined as one-third of the trace of the orthogonalized $\mathbf{U}_{ij}$ tensor.

Magnetic Susceptibility Studies. Magnetic susceptibility measurements were carried out on powders ground from selected single crystals. A Quantum Design MPMS5 SQUID magnetometer was used to collect data from 3 to 300 K. Variable-temperature data was collected at a field of 2000 G. Field dependence studies were carried out at 3 K, with the applied field varied from 0 to 55 000 G, the maximum field available. Faceted crystals of $Dy_2AuAl_6Si_4$ were found with clearly defined axial directions. The orientation dependence of the magnetic susceptibility was investigated by aligning these crystals with the a- or c-axis alternately along the magnetic field and collecting temperature dependence and field dependence data.

(8) *SAINT*, version 4; Siemens Analytical X-ray Instruments Inc.: Madison, WI, 1995.

(9) Sheldrick, G. M. *SHELXTL. Structure Determination Programs*, version 5.0; Siemens Analytical X-ray Instruments Inc.: Madison, WI, 1995. (b) *SADABS*; University of Gottingen: Gottingen, Germany, 1995.

Table 3. Selected Bond Lengths (Å) for $RE_2MAl_6Si_4$ Compounds

bond	$Gd_2PtAl_6Si_4$ (**1**)	$Gd_2AuAl_6Si_4$(**2**)	$Tb_2PtAl_6Si_4$(**3**)	$Tb_2AuAl_6Si_4$(**4**)	$Dy_2PtAl_6Si_4$(**5**)	$Dy_2AuAl_6Si_4$(**6**)
RE−Si(1) × 3	2.993(3)	2.979(1)	2.979(1)	2.9727(8)	2.965(2)	2.964(2)
RE−Si(2) × 3	2.950(2)	2.962(1)	2.938(1)	2.9519(8)	2.921(2)	2.946(2)
M−Al(3) × 6	2.522(2)	2.5424(8)	2.5234(9)	2.5485(5)	2.516(1)	2.552(1)
M−Al(2) × 2	2.535(5)	2.594(2)	2.548(3)	2.599(2)	2.527(3)	2.600(3)
Al(1)−Si(1) × 3	2.493(2)	2.4934(9)	2.493(1)	2.4999(6)	2.488(1)	2.504(1)
Al(1)−Si(1) × 1	2.547(6)	2.528(3)	2.559(4)	2.531(2)	2.543(5)	2.536(4)
Al(2)−Si(2) × 3	2.557(2)	2.534(1)	2.551(1)	2.5423(7)	2.556(2)	2.547(2)
Al(3)−Si(2) × 1	2.645(6)	2.568(3)	2.633(3)	2.580(2)	2.650(4)	2.585(4)

Band Structure Calculations. The electronic structure calculations for $RE_2MAl_6Si_4$ were performed using the self-consistent full-potential linearized augmented plane wave method (LAPW) within density functional theory (DFT);[10] the WIEN2K program was used.[11] The generalized gradient approximation (GGA) of Perdew, Burke, and Ernzerhof was used for the exchange and correlation potential.[12] To avoid the difficulties associated with the presence of incomplete f-shells in such calculations, $Lu_2PtAl_6Si_4$ was used as the model compound. The values of the atomic radii were taken to be 2.2 au for Al atoms, 2.3 au for Si, and 2.5 au for Pt and Lu atoms, where au is the atomic unit (0.529 Å). Convergence of the self-consistent iterations was performed for 19 k points in the reduced Brillouin zone with a cutoff between valence and core states of −6.0 Ry; the applied $R_{min}K_{max}$ value was 8. Convergence was assumed when the total energy difference between cycles was within 0.0001 Ry. Scalar relativistic corrections were included, and spin−orbit interaction was incorporated using a second variational procedure.[13]

Results and Discussion

Synthesis. The $RE_2MAl_6Si_4$ phase forms within a product-rich synthesis space. Initial investigations into the (Gd, Tb, or Dy)/(Au or Pt)/Al/Si system using a 1:1:10:5 reactant ratio led to a variety of crystalline products isolated from the liquid aluminum, which in all cases included $REAlSi_2$, $REAl_2Si_2$, and $RE_2MAl_6Si_4$ phases. Use of Gd as the rare earth and gold as the transition metal also produced platelike crystals of tetragonal $GdAu_4Al_8Si$, a structure that forms with early rare earth elements (Ce−Gd).[14] In the Tb- and Dy-containing reactions with Au, byproducts included recrystallized gold and $REAu_3Al_7$.[15] Platinum reactions resulted in $RE_{0.67}Pt_2Al_4Si$ as an additional product.[16]

Modifying the reactant ratio did not increase the yield of the $RE_2MAl_6Si_4$ phase. A ratio of 2:1:10:5 produced only a small amount of $RE_2MAl_6Si_4$ but drastically increased the yields of binary and ternary RE/Al/Si compounds. It is notable that reactant ratios with lower amounts of silicon do not yield any $RE_2MAl_6Si_4$ or the two ternary compounds $REAlSi_2$ and $REAl_2Si_2$. For instance, a ratio of 1:1:10:2 produced predominantly $REAl_3$ and $RE_2Al_3Si_2$,[17] with the transition metals incorporated into the ternary $REAu_3Al_7$ for the gold reactions and the quaternary $RE_{0.67}Pt_2Al_4Si$ for reactions with platinum. It is possible that increased yields of $RE_2MAl_6Si_4$ might be achieved by modifying the heating profile. The one used in this work was designed for exploratory synthesis of intermetallics and therefore incorporates a number of steps which could promote crystallization; it may not be optimal for the title compounds.

The $RE_2AuAl_6Si_4$ compounds form large, platelike crystals with evident trigonal symmetry; an example is shown in Figure 1a. The platinum-containing analogues, on the other hand, tend to form as ill-defined chunks. All $RE_2MAl_6Si_4$ phases have metallic luster, with the gold compounds showing a slight yellowish tinge. As mentioned above, the yields of these materials are very low, under 10% in all cases (based on rare-earth reactant). They are stable in air and in 5 M NaOH but are slowly attacked by 5 M HCl.

A silicon-rich flux is evidently required for the formation of $REAlSi_2$, $REAl_2Si_2$, and the title compound $RE_2MAl_6Si_4$. As the discussion below will indicate, these three structures are related. All three feature hexagonal nets of rare-earth ions sandwiched between puckered AlSi layers. The structural similarity between these compounds is mirrored in their similar synthesis characteristics, with all three often growing in the same reaction. Physical intergrowth of their crystals, as shown in Figure 1b,c, is also facilitated by the presence of similar structural motifs.

Structure. The structure of $RE_2MAl_6Si_4$ is shown in Figure 2. The two kinds of layers present in the structure, $REAl_2Si_2$-type and $RENiAl_4Ge_2$-type, are highlighted to show that this compound can be expressed as $RE_2[Al_2Si_2][MAl_4Si_2]$. The Al_2Si_2 moiety consists of a bilayer of puckered hexagonal arrays of alternating Al and Si atoms stacked along the *c*-axis and linked through Al−Si bonds; see Figure 3. Four silicon atoms surround each aluminum atom in a roughly tetrahedral arrangement. The silicon atoms comprise the capping sites of this layer, coordinated to three "equatorial" aluminum atoms and one "axial" aluminum atom in an umbrella-like fashion. The parent compound of this structural motif is $CaAl_2Si_2$; this and other analogues containing divalent ions (Sr, Eu) can be thought of in charge balancing

(10) Hohenberg, P.; Kohn, W. *Phys. Rev*. **1964**, *136*, B864. (b) Kohn, W.; Sham, L. *Phys. Rev.* **1965**, *140*, A1133. (c) Singh, D. *Planewaves, Pseudopotentials, and the LAPW Method*; Kluwer Academic: Boston, MA, 1994.
(11) Blaha, P.; Schwarz, K.; Madsen, G.; Kvasnicka, D.; Luitz, J. *WIEN2K, an Augmented Plane Wave + Local Orbitals Program for calculating crystal properties*; Schwarz, Karlheinz, Ed.; Techn. Universität: Wien, Austria, 2001.
(12) Perdew, J. P.; Burke, K.; Ernzerhof, M. *Phys. Rev. Lett*. **1996**, *77*, 3865.
(13) Koelling, D. D.; Harmon, B. *J. Phys. C* **1980**, *13*, 6147.
(14) Latturner, S. E.; Bilc, D.; Mahanti, S. D.; Kanatzidis, M. G. *Chem. Commun*. **2003**, *18*, 2340.
(15) Latturner, S. E.; Bilc, D.; Ireland, J.; Kannewurf, C.; Mahanti, S. D.; Kanatzidis, M.G. *J. Solid State Chem.* **2003**, *170*, 48.
(16) Latturner, S. E.; Kanatzidis, M. G. *Inorg. Chem*. **2002**, *41*, 5479−5486.
(17) Yanson, T.; Manyakov, M.; Bodak, O.; Gladyshevskii, R.; Cerny, R.; Yvon, K. *Acta Crystallogr. C* **1994**, *50*, 1377. (b) Chen, X.; Sieve, B.; Henning, R.; Schultz, A. Brazis, P.; Kannewurf, C.; Cowen, J. Crosby, R.; Kanatzidis, M. *Angew. Chem., Int. Ed.* **1999**, *38*, 693.

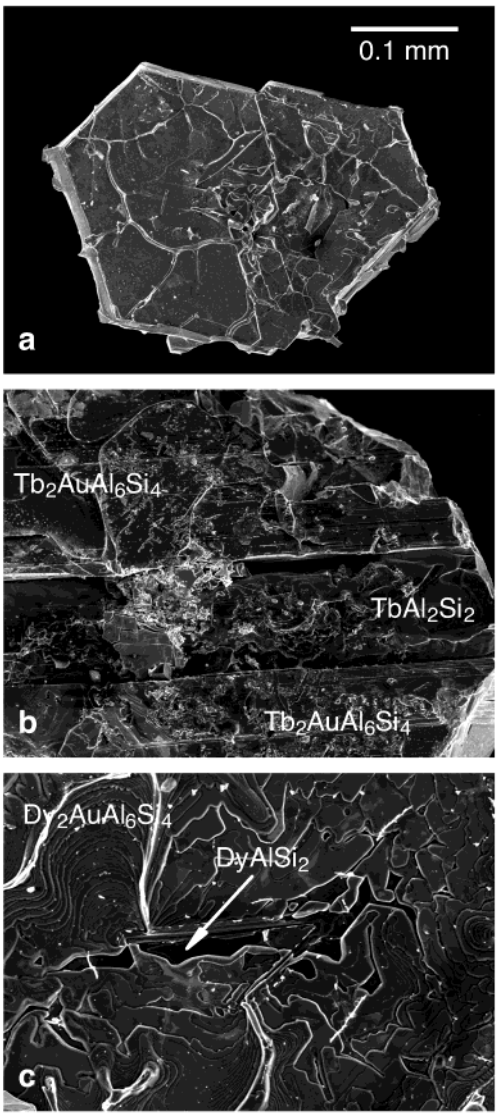

Figure 1. Scanning electron micrographs of $RE_2MAl_6Si_4$ products: (a) a large twinned crystal of $Dy_2AuAl_6Si_4$, showing the trigonal symmetry of the structure; (b) a layer of $TbAl_2Si_2$ is sandwiched between two crystals of $Tb_2AuAl_6Si_4$; (c) a coating of $Dy_2AuAl_6Si_4$ growing on top of a crystal of $DyAlSi_2$. Note the trigonal symmetry of the growth steps.

terms as $Ca^{2+}(Al^{3+})_2(Si^{4-})_2$. Because of this, the discovery that this structure also forms with certain trivalent rare-earth ions was somewhat surprising. $REAl_2Si_2$ forms in trigonal space group $P\bar{3}m1$ with RE = Y, Sm, Eu, Gd, Tb, Dy, and Yb; the unit cell parameters range between 4.15 and 4.20 Å for *a* (the same range is observed for the $RE_2MAl_6Si_4$ compounds; see Table 1) and 6.58−6.91 Å for *c*.[18,19] $GdAl_2Si_2$, $TbAl_2Si_2$, and $DyAl_2Si_2$ were found as byproducts of the reactions studied in this work, as was $REAlSi_2$ (an intergrowth structure of $REAl_2Si_2$ slabs and AlB_2-type Si net layers).[20] The existence of the isostructural pair of $CaAl_2Si_2$ and $REAl_2Si_2$ implies that alkaline-earth analogues (such as $Ca_2MAl_6Si_4$) or mixed rare-earth/alkaline-earth analogues (such as $(RE/Ca)_2MAl_6Si_4$) of the title compound may also be stable.

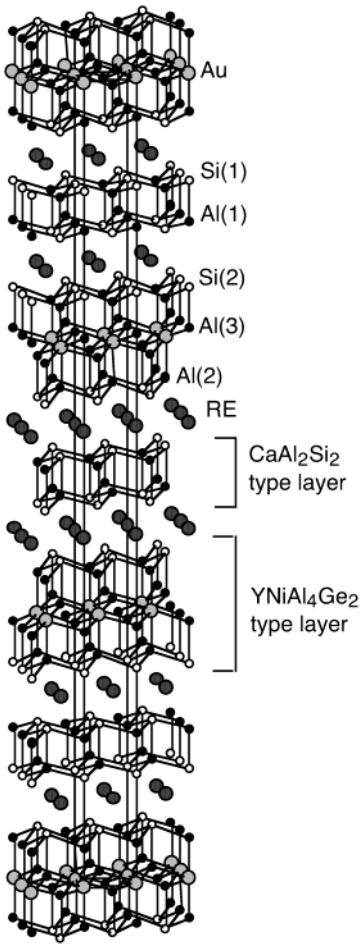

Figure 2. $RE_2MAl_6Si_4$ structure. The $CaAl_2Si_2$ and $YNiAl_4Ge_2$ type slabs are highlighted.

Prior investigations into $REAl_2Si_2$ have explored the bonding within each puckered AlSi layer and that between the layers which links them together. The equatorial bonds (the three Al−Si bonds in roughly the *ab* plane) were found to be shorter than the single Al−Si axial bond in the *c* direction.[19] As shown in Table 3, this is also the case for $RE_2MAl_6Si_4$. The importance of this will be disclosed in the band structure calculations.

The transition metal-containing slab is the same moiety found in the $YNiAl_4Ge_2$ structure.[4] Investigations into RE/(Au or Pt)/Al/Si quaternaries grown in aluminum flux indicate that gold and platinum appear to favor different coordination environments. Several quaternary compounds have been discovered with gold and aluminum forming antifluorite type slabs similar to the bulk $AuAl_2$ structure.[14,21] Platinum, on the other hand, appears to favor a stuffed arsenic coordination as found in $Gd_{1.33}Pt_3Al_7Si$ and $RE_{0.67}Pt_2Al_4Si$. It is therefore surprising that both noble metals form the same structure; however, as Figure 3 indicates, the RE_2(Au or Pt)Al_6Si_4 structure type combines aspects of the antifluorite

(18) Villars, P. *Pearson's Handbook, Desk Edition: Crystallographic Data for Intermetallic Phases, Vol. 1*; ASM International: Materials Park, OH, 1997.
(19) Kranenberg, C.; Johrendt, D.; Mewis, A. *Z. Anorg. Allg. Chem.* **1999**, *625*, 1787−1793.
(20) Kranenberg, C.; Johrendt, D.; Mewis, A.; Kockelmann, W. *Z. Naturforsch.* **2001**, *56B*, 620−625.
(21) Latturner, S. E.; Bilc, D.; Mahanti, S. D.; Kanatzidis, M. G. *Chem. Mater.* **2002**, *14*, 1695−1705.

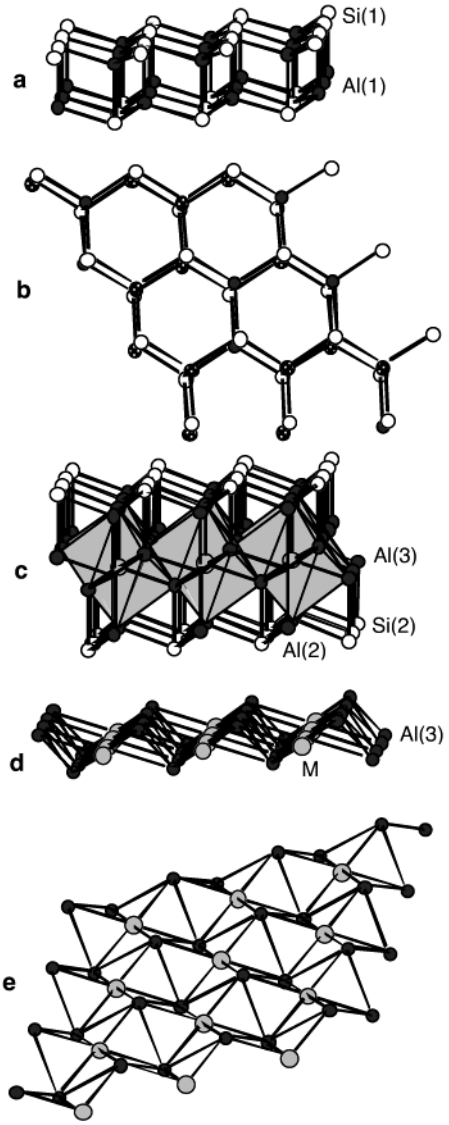

Figure 3. Details of the slabs within the $RE_2MAl_6Si_4$ structure: (a) $CaAl_2Si_2$-type slab, viewed along the *a*-axis; (b) $CaAl_2Si_2$ slab, viewed down the *c*-axis; (c) $YNiAl_4Ge_2$-type slab, showing the MAl_8 cubes; (d) a layer that can also be thought of as a MAl_2 layer sandwiched between two AlSi capping layers (not shown), where the MAl_2 layer has the same stuffed arsenic configuration observed in $Gd_{1.33}Pt_3Al_7Si$;[16] (e) oblique view of the MAl_2 layer, showing the puckering of this layer.

$AuAl_2$ arrangement and the stuffed arsenic coordination. This MAl_4Si_2 layer allows for both transition metals to assume a coordination environment favorable to them.

In Figure 3c, the roughly cubic distribution of eight aluminum atoms around each transition metal atom is highlighted. This is the same coordination environment observed for gold in the antifluorite $AuAl_2$ structure and in many RE/Au/Al/Si quaternary compounds. As indicated by the bond lengths in Table 3, the cube is somewhat distorted, with 6 M−Al(3) bonds of identical length and two longer M−Al(2) bonds in the *c*-axis direction. This may indicate that the slab is better viewed as a stuffed arsenic MAl_2 layer, capped above and below by two puckered AlSi sheets. Figure 3d,e highlights this aspect, showing the transition metal in the center of a chair conformation cyclohexane-like ring of six aluminum atoms.

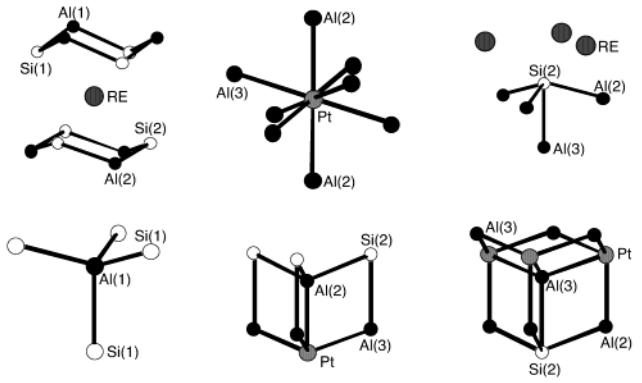

Figure 4. Local coordination environments of the atoms in $RE_2MAl_6Si_4$. Si(1) and Si(2) have similar environments so only Si(2) is shown.

Table 4. Magnetic Susceptibility Data for $RE_2MAl_6Si_4$ Compounds

compd	T_N (K)	exptl μ_{eff} (μ_B)	theor μ_{eff} (μ_B)	θ (K)	comments
$Gd_2PtAl_6Si_4$	14.0	7.85	7.94	−15.5	
$Gd_2AuAl_6Si_4$	20.0	7.77	7.94	−19.2	
$Tb_2PtAl_6Si_4$	8.0	9.40	9.72	−4.9	
$Tb_2AuAl_6Si_4$	14.5	9.38	9.72	−22.2	
$Dy_2PtAl_6Si_4$	7.5	10.56	10.65	+0.14	metamagnetic
$Dy_2AuAl_6Si_4$	10.0	10.79	10.65	+2.54	metamagnetic

Puckered AlSi sheets serve as the outer layers of both the Al_2Si_2 and MAl_4Si_2 slabs and, therefore, provide an all-silicon coordination environment for the rare-earth cations in $RE_2MAl_6Si_4$. Six capping silicon atoms coordinate each rare-earth ion in a roughly octahedral fashion, as shown in Figure 4. The RE's are slightly closer to the Si atoms of the MAl_4Si_2 layer than those of the Al_2Si_2 layer. This can be understood given the more electron-rich nature of the MAl_4Si_2 slab; it contains the late transition metal, as well as the capping silicon atoms.

Magnetic Characterization. All the $RE_2MAl_6Si_4$ compounds display paramagnetic behavior at high temperatures. The data can be fit using the Curie−Weiss relationship; the magnetic moments per RE^{3+} ion derived from the data are in agreement with the theoretical values for Gd^{3+}, Tb^{3+}, and Dy^{3+} (see Table 4). This indicates that platinum and gold are diamagnetic, in agreement with their high electronegativity. The late transition metals are in fact the most electronegative elements in the structure, followed by silicon. Electrons are transferred from the more electropositive elements in the structure (the rare-earth elements) to these transition metals and to silicon. This results in the filling of the d-orbitals of gold or platinum and diamagnetic behavior for these atoms; this is a commonly seen phenomenon in late transition metal intermetallic compounds.[1a]

Antiferromagnetic ordering is observed for all six phases at low temperature; see Figure 5. The identity of the rare earth appears to have the biggest influence on the magnetic behavior at and below T_N, although, for each RE, the gold-containing compound has a higher Neel temperature than the platinum analogue. The gadolinium phases have a broad transition to antiferromagnetic order, with a higher T_N on average than the terbium analogues (which in turn have a higher T_N than the Dy phases). The magnetization behavior at 3 K for $Gd_2MAl_6Si_4$ is linear, showing no sign of saturation

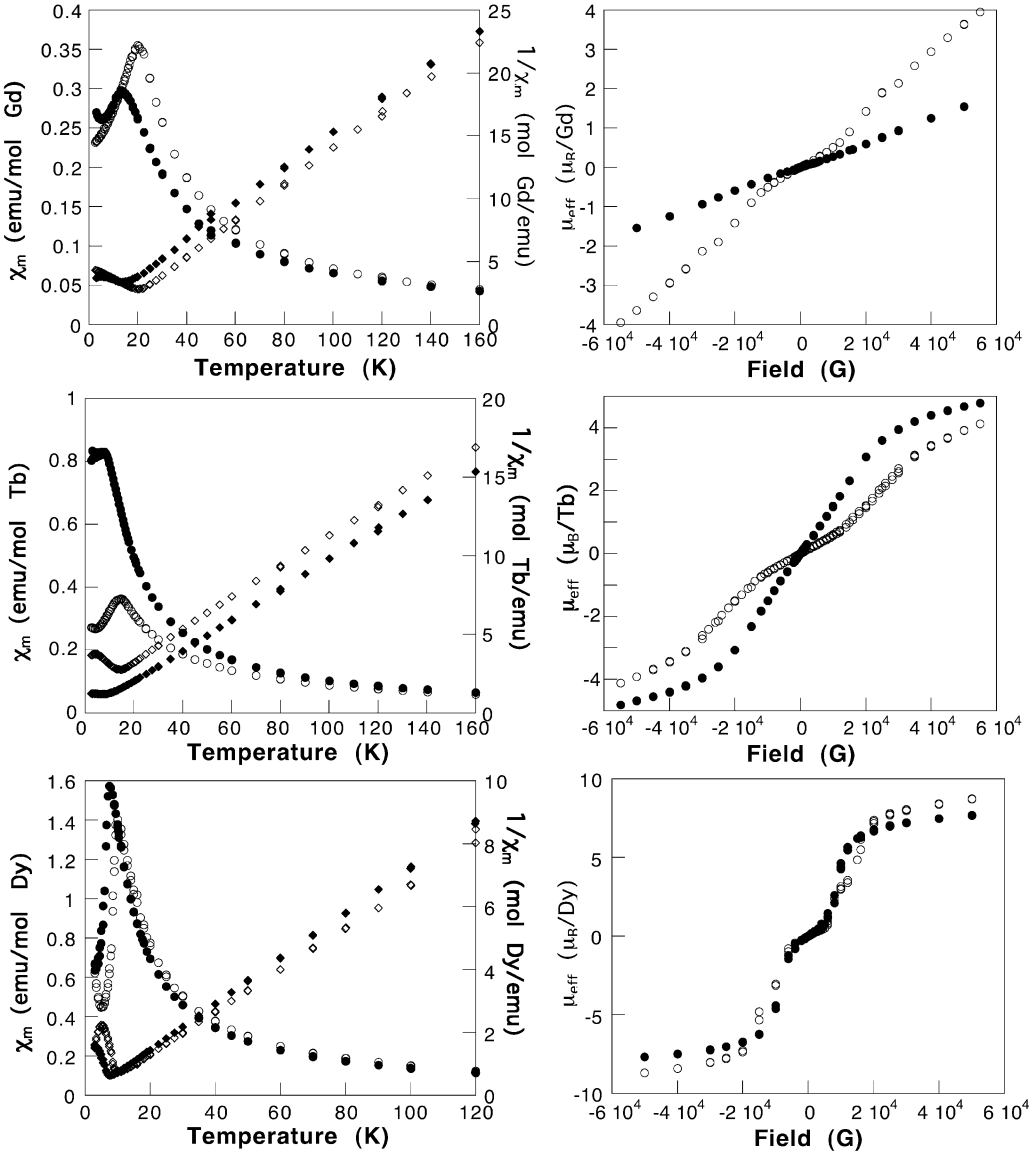

Figure 5. Magnetic susceptibility data for $RE_2MAl_6Si_4$ compounds. For each rare-earth data set, open circles correspond to the platinum analogue and filled circles to the gold analogue.

at the highest field available. The terbium compounds also show a broad antiferromagnetic transition, but their magnetization behavior is slightly more complex. There is no evidence of complete metamagnetic ordering or saturation, but the kinks in the data indicate some slight reorientation of spins as the field is varied.

$Dy_2AuAl_6Si_4$ and $Dy_2PtAl_6Si_4$ both show a sharp transition to antiferromagnetic order at around 10 K and metamagnetic behavior at 3 K. The dependence of the magnetization on field at 3 K is roughly linear up to a field of 6000 G, where a spin reorientation begins to occur. This is perhaps a switch to a more ferromagnetic arrangement of the magnetic moments, since the magnetization begins to saturate above 20 000 G at values approaching the theoretical maximum for Dy^{3+}. The positive sign of the Weiss constants for the dysprosium phases also points to the existence of ferromagnetic correlations. The metamagnetic spin reorientation appears to happen in two steps for $Dy_2AuAl_6Si_4$. Another indication of slightly more complex magnetic behavior for the gold compound is apparent in the temperature dependence of χ_m, which has an upswing at 5 K (below the antiferromagnetic transition temperature); a similar transition is not seen in the data for the Pt analogue.

Further investigation of $Dy_2AuAl_6Si_4$ was carried out on single crystals of this material. The temperature dependence of the susceptibility and the magnetization behavior at 3 K were studied in two orientations—for one, the *a*-axis was aligned with the magnetic field; for the other, the *c*-axis was aligned along the field. The results are shown in Figure 6. It is immediately evident that the spins are not antiferromagnetically ordered in a simple collinear fashion along either of these axes, since the expected precipitous drop off of "$\chi_{||}$" and the leveling off of "$\chi_{\perp}$" below T_N is not observed.

The magnetization behavior of $Dy_2AuAl_6Si_4$ shows a more obvious orientation dependence. H_C (the field at which the metamagnetic spin reorientation occurs) is 5000 G with the *a*-axis parallel to the magnetic field. When the *c*-axis is directed along the field, H_c is raised to 8000 G. These H_c

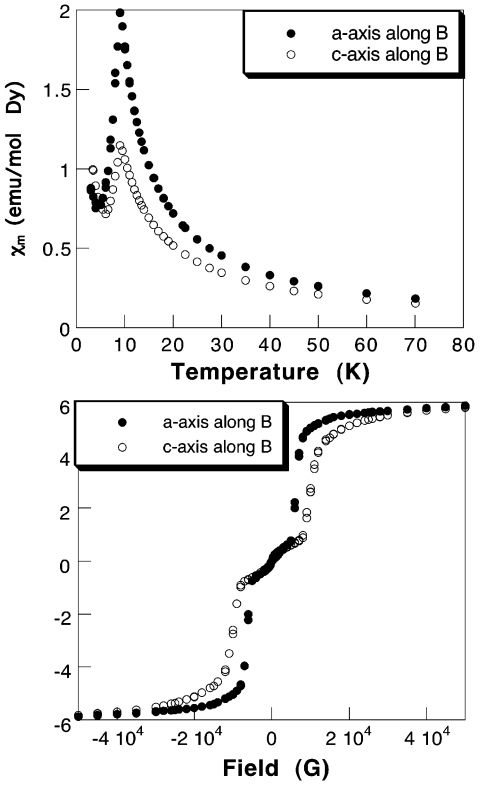

Figure 6. Orientation dependence of the magnetic susceptibility for $Dy_2AuAl_6Si_4$.

values bracket the critical field of 6000 G observed for the isotropic powder sample. The magnetic saturation values at high fields are identical in both orientations. This is another indication of a complex arrangement of spins; if there is a clear magnetic "easy axis" near or along the *a*- or *c*-axis of the crystal, the saturation should be higher when the field is directed along this axis. A possible contributing factor to the spin complexity is the trigonal arrangement of rare-earth ions in the structure, which can create frustration in antiferromagnetic coupling.[22] Preliminary ac susceptibility measurements did not show any evidence of spin glass behavior, however. Neutron scattering data is likely required to shed more light on this situation.

Band Structure. Band structure calculations were carried out to further investigate the electronic characteristics of the $RE_2MAl_6Si_4$ phases. The total density of states (DOS) data for the hypothetical model compound $Lu_2PtAl_6Si_4$ and partial density of states diagrams for selected atoms in the structure are shown in Figure 7; additional band structure diagrams may be found in the Supporting Information. The main features are the two sharp f-bands of lutetium at −5 and −6.5 below the Fermi level (split by spin−orbit coupling) and the envelope of Pt d-orbitals in this same energy region. The low-energy, filled Pt d-shell is in agreement with the magnetic susceptibility data and with the behavior of other late transition metal-containing intermetallics.[1a] Another characteristic of the density of states for this structure is a pseudogap at E_f. This is also observed in other polar intermetallic materials and has been ascribed to strong

(22) Gignoux, D.; Schmitt, D. *J. Alloys Compd.* **2001**, *326*, 143−150.

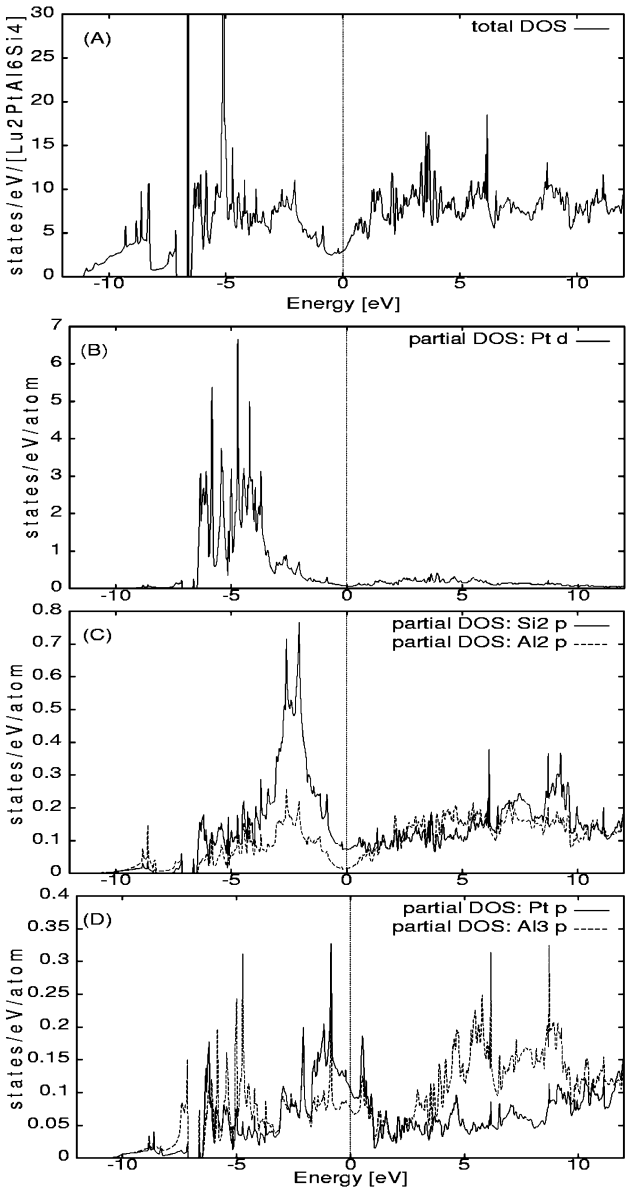

Figure 7. Density of states data for $Lu_2PtAl_6Si_4$, where the Fermi level is at 0 eV: (a) total density of states with the sharp Lu f-bands truncated to allow detail near E_f to be visible; (b) partial DOS for the Pt d-orbitals; (c) partial DOS for the p-orbitals of the atoms in the capping AlSi sheet of the $PtAl_4Si_2$ slab, Si(2) and Al(2); (d) partial DOS for the p-orbitals of Pt and Al(3), the atoms that comprise the $PtAl_2$ stuffed arsenic type layer.

covalent-type bonding in the network surrounding the electropositive cations. The presence of "bonding" levels below E_f and "antibonding" states above E_f (as shown by COOP calculations on several intermetallics) indicates a somewhat localized bonding description may be appropriate.[1b] Further investigation into details of the band structure supports this, revealing that the 3-dimensional slabs in the $RE_2MAl_6Si_4$ structure contain electronically distinct layers.[23]

The contributions of Pt, Al(3), Al(2), and Si(2) orbitals to the density of states are shown in Figure 7b−d. It is evident that the atoms comprising the stuffed arsenic layer (Pt and

(23) Similar band structure calculations were carried out on the hypothetical gold analogue $Lu_2AuAl_6Si_4$. The same characteristics were observed; the Fermi level was higher due to the additional electron but still fell in the pseudogap region.

Al(3)) contribute to bands that are not hybridized with bands resulting from the combination of Si(2) and Al(2) orbitals. The stuffed arsenic layer $PtAl_2$ thus appears to exist as an almost separate electronic entity from the capping puckered AlSi layers surrounding it in the $YNiAl_4Ge_2$ type slab. This is also evident to some extent in the bond distances in Table 3; Si(2)−Al(2) is shorter than Si(2)−Al(3), and Pt has a shorter bond to the Al(3) in the stuffed arsenic slab compared to the bond to Al(2). The $PtAl_2$ hybridized bands show a significant DOS across the Fermi level and may be responsible for the bulk of the conductivity in the structure.

Orbitals of the Al(2) and Si(2) atoms that comprise the AlSi nets in the $PtAl_4Si_2$ slab hybridize to form several highly dispersed bands. The Al(2)−Si(2) bands just below the Fermi level show a larger contribution from Si than Al; bands above the pseudogap have a larger Al component. This is in line with electronegativity considerations. The bands derived from the hybridization of Al(1) and Si(1) (the atoms comprising the Al_2Si_2 slab; data not shown) have similar shape and behavior. The silicon atoms Si(1) and Si(2) also make the largest contributions to somewhat flat bands just below the Fermi level; these bands likely originate from the nonbonding electron pairs on these capping atoms. This is in agreement with previous calculations on $CaAl_2Si_2$, which show Si lone pair orbitals at the top of the valence band.[24]

This leads to the possibility that each puckered AlSi layer can be thought of as a possibly independent entity. Due to the symmetry of the structure, the AlSi layers in the $CaAl_2Si_2$ type slab of $Lu_2PtAl_6Si_4$ cannot be distinguished from each other in the band structure. However, as previously mentioned, inspection of the bond distances shows a longer axial Al−Si bond between these layers compared to the shorter equatorial Si−Al bonds within the layers. This has also been observed in the Al_2Si_2 slabs of $CaAl_2Si_2$ and $LaAlSi_2$.[19,20] Band structure studies carried out on these ternary compounds indicate that s−p hybridization at the Si capping site decreases the sp overlap in the axial Al−Si bonds as it produces "lone pair" orbitals on the Si atom which point toward the hexagonal net of cations.[24] Electron localization function (ELF) calculations carried out on $LaAlSi_2$ confirm that the Al_2Si_2 slab can be considered as a stacking of two AlSi nets, with the electron density in the equatorial Al−Si bonds much greater than that in the axial Al−Si bond.[20] Because of the relatively electronically isolated nature of these layers, the transport properties of all compounds containing AlSi nets are expected to be highly anisotropic.

Concluding Remarks

The reaction of a rare-earth element with noble metals gold or platinum in a silicon-rich aluminum flux produces the quaternary intermetallic compounds $RE_2MAl_6Si_4$. These possess a new structure comprised of $CaAl_2Si_2$-type layers and $YNiAl_4Ge_2$-type layers. The Al_2Si_2 structural moiety in these compounds is also observed in the ternary byproducts of this reaction, $REAl_2Si_2$ and $REAlSi_2$. These compounds are not formed in reactions with lower amounts of silicon, indicating that a high concentration of Si in the molten aluminum solution is necessary to promote the growth of Al_2Si_2 slabs. The AlSi puckered hexagonal sheets that comprise this slab are also found in the other building block of the structure, the MAl_4Si_2 layer. Band structure calculations indicate that these sheets may give rise to highly anisotropic electronic properties.

Acknowledgment. Financial support from the Department of Energy (Grant DE-FG02-99E45793) is gratefully acknowledged. This work made use of the SEM facilities of the Center for Electron Optics at Michigan State University.

Supporting Information Available: Additional crystallographic data such as atomic positions, anisotropic displacement parameters, and bond distances and angles for all compounds as CIF files and band structure diagrams for $Lu_2PtAl_6Si_4$ (drawn in fat band representation to show contributions of Pt, Al(2), Al(3), and Si(2) orbitals). This material is available free of charge via the Internet at http://pubs.acs.org.

IC0346432

(24) Burdett, J. K.; Miller, G. J. *Chem. Mater*. **1990**, *2*, 12−26.